Draft version February 2, 2008
Preprint typeset using LaTeX style emulateapj v. 6/22/04

A CHANDRA VIEW OF THE NORMAL S0 GALAXY NGC 1332: II: SOLAR ABUNDANCES IN THE HOT GAS AND IMPLICATIONS FOR SN ENRICHMENT.

Philip J. Humphrey[1], David A. Buote[1] and Claude R. Canizares[2]

Draft version February 2, 2008

ABSTRACT

Using a new Chandra *ACIS*-S3 observation of the normal, isolated, moderate-L_X, lenticular galaxy NGC 1332 we resolve the emission into ∼75 point-sources, and a significant diffuse component. We present a detailed analysis of the spectral properties of the diffuse emission, constraining both the temperature profile and the metal abundances in the hot gas. The characteristics of the point source population and the spatial properties of the diffuse emission are discussed in two companion papers. The diffuse component comprises hot gas, with an ∼isothermal temperature profile (∼0.5 keV), and emission from unresolved point-sources. In contrast with the cool cores of many groups and clusters, we find a small central temperature peak. We obtain emission-weighted abundance contraints within 20 kpc for several key elements: Fe, O, Ne, Mg and Si. The measured iron abundance (Z_{Fe}=1.1 in solar units; >0.53 at 99% confidence) strongly excludes the very sub-solar values often historically reported for early-type galaxies. This continues, in a lower-L_X system, a trend in recent observations of bright galaxies and groups. The abundance ratios, with respect to Fe, of the other elements were also found to be ∼solar, with the exception of Z_O/Z_{Fe} which was significantly lower (< 0.4), as seen in several bright galaxies, groups and clusters. Such a low O abundance is not predicted by simple models of ISM enrichment by Type Ia and Type II supernovae, and may indicate a significant contribution from primordial hypernovae. Revisiting *Chandra* observations of the moderate-L_X, isolated elliptical NGC 720, we obtain similar abundance constraints ($Z_{Fe}=0.71^{+0.40}_{-0.21}$, 90% confidence; $Z_O/Z_{Fe}=0.23\pm0.21$). Adopting standard SNIa and SNII metal yield models, our abundance ratio constraints imply 73±5% and 85±6% of the Fe enrichment in NGC 1332 and NGC 720, respectively, arises from SNIa. Although these results are sensitive to the considerable systematic uncertainty in the SNe yields, they are in good agreement with observations of more massive systems. These two cases of moderate-L_X early-type galaxies reveal a consistent pattern of metal enrichment from cluster scales to moderate L_X/L_B galaxies.

Subject headings: Xrays: galaxies— galaxies: elliptical and lenticular, cD— galaxies: abundances— galaxies: individual(NGC 1332)— galaxies: halos— galaxies: ISM

1. INTRODUCTION

During the formation and evolution of early-type galaxies, the primordial gas is enriched by supernovae ejecta and stellar mass-loss. Observations of the metal content of the hot, X-ray emitting gas within such galaxies therefore offer a powerful means to investigate their history (e.g. Loewenstein & Mathews 1991). In early *ASCA* and *Rosat* observations of early-type galaxies very sub-solar metal abundances (dominated by Fe, which has the strongest diagnostic lines in the soft X-ray band) were generally reported (e.g. Davis & White 1996; Mulchaey & Zabludoff 1998; Loewenstein & Mushotzky 1998; Matsumoto et al. 1997; Matsushita et al. 1994). In stark contrast, the mean stellar iron abundance in elliptical galaxies tends to be ∼solar (Arimoto et al. 1997), implying that the ISM could not have been substantially enriched by SNIa and mass-loss from the stellar population. However, the mean iron abundances determined by X-ray observations of clusters tend to be ∼0.3–0.5 times solar, requiring significant enrichment of the primordial gas, most probably from the stellar population of the giant elliptical galaxies (Renzini 1997). This discrepancy is problematical, as it is difficult to envisage how individual early-type galaxies could have, in many cases, *lower* iron abundances than typical clusters. Indeed, gas enrichment models for the centres of individual galaxies tend to predict super-solar values of Z_{Fe} (e.g. Ciotti et al. 1991; Loewenstein & Mathews 1991; Brighenti & Mathews 1999). This obvious inconsistency led Arimoto et al. (1997) to question the validity of the X-ray plasma codes which were being fitted to the data, especially given uncertainties in the physics of the Fe L-shell transitions.

An alternative explanation was provided by Buote & Fabian (1998), who demonstrated that fitting a single temperature model to intrinsically non-isothermal data can give rise to an "Fe bias", in which the iron abundance is systematically under-estimated, and instead obtained ∼solar abundances by fitting multi-temperature models to a variety of bright elliptical galaxies (see also Buote 2000b and e.g. Buote et al. 2003b, who found comparable results with different plasma models). Although it had long been recognized that a hard spectral component (to account for unresolved point source emission) was required to fit the *ASCA* data of many early-type galaxies (Matsushita et al. 1994), the spectral shape of this component is much harder (kT$\gtrsim$5 keV) than the hot gas emission (for which kT∼0.5–1.0 keV), so that it cannot move to mitigate, even in part, the Fe bias. Nonetheless,

[1] Department of Physics and Astronomy, University of California at Irvine, 4129 Frederick Reines Hall, Irvine, CA 92697-4575
[2] Department of Physics and Center for Space Research, 37-241 Massachusetts Institute of Technology, 77 Massachusetts Avenue, Cambridge, MA 02139

Buote & Fabian (1998) still found that, in the lower-L_X systems, in which the data were consistent with a *single* hot gas component plus unresolved sources, the abundances were consistent with $Z_{Fe}\simeq1$. However, the lower signal-to-noise resulted in very poor constraints so that very sub-solar Z_{Fe} values could often not be entirely ruled out. A similar result for a low S/N system was reported by Kim et al. (1996) for the low L_X/L_B S0 NGC 4382 observed with *ASCA*.

More recent *Chandra* and *XMM* observations of bright ellipticals and the centres of bright groups have tended to confirm near solar (or even super-solar) abundances (e.g. NGC 5044:Buote et al. 2003b,Tamura et al. 2003; M 87: Gastaldello & Molendi 2002; NGC 1399: Buote 2002; NGC 4636: Xu et al. 2002; MKW 4: O'Sullivan et al. 2003; also c.f. the low L_X/L_B radio galaxy NGC 1316: Kim & Fabbiano 2003). However, for some systems, especially (but not exclusively) the lowest-L_X/L_B galaxies, authors are still tending to find very sub-solar metal abundances (e.g. NGC 1291: Irwin et al. 2002, NGC 4697: Sarazin et al. 2001; especially NGC 3585, NGC 4494 and NGC 5322, for which $Z_{Fe}\lesssim0.1$ was reported by O'Sullivan & Ponman 2004; also c.f. the X-ray bright radio galaxy NGC 6251: Sambruna et al. 2004).

The lack of a consistent picture of enrichment from galaxy to cluster scales is a major problem in our understanding of galaxy evolution. It is therefore of critical importance to determine accurate abundances in galaxies with a wide range of L_X/L_B, and especially to determine the ubiquity of the very sub-solar abundances in low-L_X/L_B systems. In this paper, we present a *Chandra* study of the metal abundances in the hot gas of the "normal", relatively isolated, moderate-L_X lenticular galaxy NGC 1332. In two companion papers (Humphrey & Buote 2004; Buote et al. 2004, hereafter Paper I and Paper III), we present a study of the X-ray point-source population and the gravitating matter distribution, which have been able to take advantage of the excellent spatial resolution of *Chandra*.

NGC 1332 has a much lower L_X (and L_X/L_B) than most of the gas-rich giant elliptical galaxies for which ∼solar abundances have been found. Furthermore, its L_X/L_B is sufficiently high to ensure substantial emission from the hot gas. For many systems with much lower L_X/L_B, such analysis is hampered by a lack of photons (which may introduce abundance degeneracies or extremely poor constraints; c.f. Buote & Fabian 1998). Significant diffuse gas emission in NGC 1332 was inferred from previous X-ray observations, making it an ideal subject for such a study. Using *Rosat* PSPC observations, Buote & Canizares (1996) found evidence of a flattened dark matter halo in NGC 1332. Although the *ASCA* data enabled the unambiguous identification of a hard spectral component (supposed to arise from unresolved point sources), the signal-to-noise was insufficient to enable good constraints on the metal abundances to be determined (Buote & Fabian 1998) (rescaling to the new solar abundances, these authors found $Z_{Fe}> 0.3$). Although the best-fit value ($Z_{Fe}\simeq1.2$) was clearly consistent with ∼solar abundances, highly subsolar values could not be excluded.

Throughout this paper, we adopt the new standard abundances of Grevesse & Sauval (1998). We note that there is some complication in comparing to the literature as many authors still use the outdated solar abundances of Anders & Grevesse (1989). Although we quote all abundances with respect to the new standard, the most significant discrepancy between fits using the two standards is a difference in the inferred value of Z_{Fe}; for comparison with our work, Z_{Fe} determined using the older abundances should be multiplied by ∼1.5. All quoted confidence regions are 90%, unless otherwise stated.

2. BACKGROUND AND FLARING

The region of sky containing NGC 1332 was observed with the ACIS instrument aboard *Chandra* between 2002 September 19 10:39 and September 20 02:59 UTC, the galaxy being centred on the S3 chip, for a nominal ∼60 ks exposure. An additional observation made between September 18 02:56 and 08:27 UTC, for a nominal 20 ks exposure, was heavily contaminated by flaring of the background and so we present results only for the better-quality dataset. We reduced and processed the data using the *CIAO* data-analysis suite of tools, version 3.0.2, and the *Chandra Caldb* version 2.26, and we performed spectral-fitting with XSPEC version 11.3.0. For a discussion of the data-reduction procedures and a detailed analysis of the point-source population in NGC 1332, we refer the interested reader to Paper I.

One of the challenges in performing analysis of relatively low surface-brightness diffuse emission is the determination of a reliable background estimate. Since the diffuse emission covers much of the S3 chip, it was not possible to determine a "local" background estimate from an appropriate region of the detector. We therefore adopted the appropriate "blank field" event files provided in the *Caldb*. There is known to be variation between different observations and different pointings in both the high and low-energy regimes of the background. This is complicated further by the "flaring" which is often observed in the background (e.g. Markevitch 2002). We therefore accumulated a background lightcurve (from 5.0–10.0 keV) from source-free regions of the active chips and examined it by eye for evidence of flaring. The lightcurve shows evidence of mild flaring activity. The strongest flares had amplitudes reaching ∼50%, but lasted for only a short fraction of the entire observation. In contrast, low-level flaring persisted through much of the observation, with an associated amplitude of ∼20%.

Completely excising the low-level flaring from the data resulted in a total exposure of only ∼28 ks. We found excellent agreement in the high-energy count-rates of the background templates and the flare-cleaned observation, indicating complete removal of the flare. However, such a short exposure unacceptably degraded the signal-to-noise level of the data. As a compromise, we excised only the periods of strongest flaring, which resulted in a more acceptable ∼45 ks exposure. We chose not to include all of the data since the significantly higher background during the remaining time periods would more than offset the signal-to-noise gain from the modest increase in exposure that would result. However, we compared spectra accumulated with each level of filtering from the same region of the S3 chip containing low surface-brightness emission from NGC 1332. The less-filtered data clearly showed significant residuals in excess of the hot gas emission at $\gtrsim2$ keV which were not seen in the more heavily-filtered data. In order to take account of this contamination, we

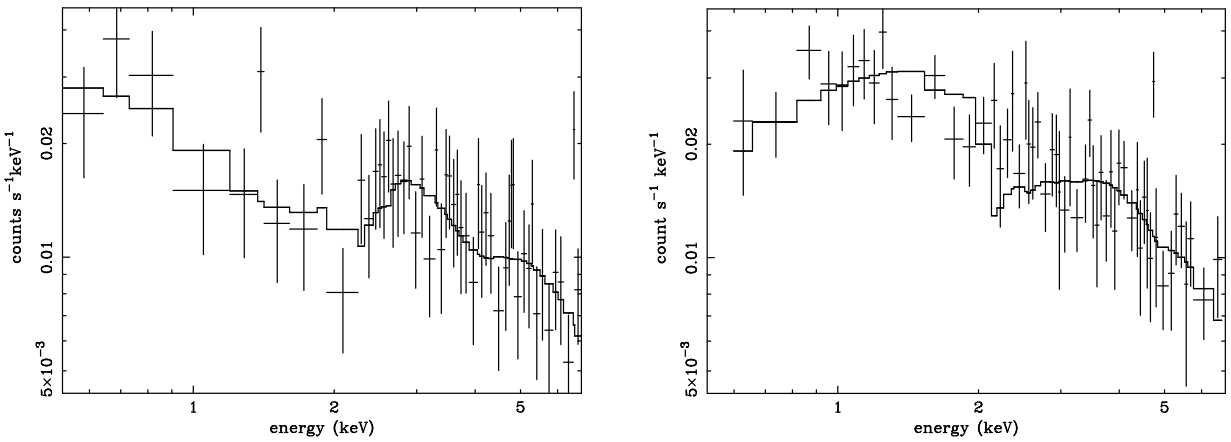

FIG. 1.— The spectra of the flaring, shown along with the best-fit models. Left panel: the flare spectrum obtained from the S3 chip. Right panel, the flare spectrum obtained from the S1 chip. Note that, since the extraction regions were not identical, we do not expect the spectral normalizations to be identical.

chose to include an additional component in our spectral-modelling. We did not attempt to renormalize the background template to match the high-energy residuals as this will also renormalize the soft X-ray background and instrumental features (which can be problematic if the flaring is sufficiently strong, as in Sect 5).

To enable us to estimate the spectral form of the flaring, it was necessary to disentangle it from the diffuse galactic emission and the X-ray background. To achieve this, we adopted two complementary techniques. Firstly, we exploited the strong variability of the flaring component, in contrast to (naturally) constant galactic emission. We accumulated a spectrum at the peak of flaring and one during a period when flaring was absent, from the same annular region from 5–160″ (excluding all photons within a region 6 times the radius of the 1σ detection region around each resolved point-source, since individual sources may be variable). The difference between these two spectra must, necessarily, be the spectrum of the flare. The two periods were chosen from the lightcurve by eye (we note that intensity-filters would not have been appropriate since the Poisson scatter, for realistic lightcurve binsizes, was not much less than the flaring amplitude). Appropriate count-weighted spectral response matrices were generated for the peak flaring data with the *CIAO* tasks **mkrmf** and **mkwarf**, and the flare-free spectrum was adopted as the background. The "flare" data were regrouped to ensure at least 20 source-plus-background photons in each spectral bin, and a signal-to-noise ratio of at least 3. This procedure assumes that the time-averaged spectrum of the flare is similar to the peak flare spectrum. A comparison of flare lightcurves accumulated in different energy bands (0.5–3.0 keV and 3.0–10.0 keV), obtained by subtracting the "quiescent" level (estimated from non-flaring stretches of data) from the background lightcurves, did not reveal any significant changes in spectral hardness during evolution of the flare. This would seem to support our assumption.

To parameterize the spectral shape of the flare we tested various spectral models against the data (which were not required to be physical). We found that the data could be very well-fitted (χ^2/dof = 41.5/46) with a broken-power law model, plus a broad gaussian term at ∼2.6 keV to soften the change in the spectral slope. In order to determine whether the flare spectrum varied with position on the S3 chip, we extracted similar spectra from the set of 5 annuli adopted in Sect 3. Excluding the two innermost annuli (for which the data were too poor for comparison), we found that the parameterized model gave an excellent fit to the data within each annulus, if the overall normalization was allowed to fit freely. The normalization scaled approximately with the extraction area, as expected for flaring which was uniform across the S3 chip.

Our alternative means of estimating the flare spectrum was to accumulate the spectrum from a source-free region of the S1 chip (since this was sufficiently offset from the galaxy centroid not to be strongly contaminated by emission from the hot gas) and account for the X-ray background by adopting the appropriate background template. We accumulated a spectrum from a region centred on the S1 chip, with a 160″ radius. We excluded data in the vicinity of a single point-source found by the detection algorithm on this chip. We extracted a background spectrum from the standard S1 "blank-fields" events file. The source spectrum was grouped to ensure there were at least 20 photons in each data bin and the signal-to-noise ratio exceeded 3. We were able to parameterize the S1 flare spectrum with a single broken power law model. There was excellent agreement between flare spectra accumulated *via* both methods above ∼2 keV (Fig 1). Between ∼1–2 keV, the flare accumulated from the S1 chip showed a significantly higher count-rate than that obtained from the S3 chip. A number of systematic effects may account for this discrepancy. Firstly, the S1 chip may not be entirely free of contamination by the diffuse emission from the galaxy. Secondly, the degradation of the PSF on the S1 due to the large offset means that point-sources may not have been detected on this chip, contaminating the data. Thirdly, the actual flare spectrum may be different between the two chips. Finally, there may be subtle differences between the background template and the actual background spectrum for our pointing. In the subsequent sections, we adopt the flaring model taken from the S3 chip, since, on balance, it

is less likely to be subject to biases than the data from the S1 chip. However, we found very little difference if the alternative flare model was used (Sect 4.4). Given the very different assumptions involved in our two estimates of the flare spectrum, this gave us confidence in our ability to model the flaring.

3. SPECTRAL ANALYSIS

For analysis of the diffuse galactic emission of NGC 1332, we extracted spectra from a single, large ($3'$) aperture and a series of contiguous, concentric annuli, all centred on the centroid of the X-ray emission. We determined the galaxy centroid self-consistently by iteratively computing the centroid in a $1'$ circle, which was re-centred at this new position, until no more refinements were required. Our initial guess for the centroid of X-ray emission was the 2MASS position given in *NED*. Our resulting position was in excellent agreement with that of the diffuse source identified at the galaxy centre by the point-source detection algorithm (Paper I) and was within $1''$ of the infra-red centroid. In order to minimize contamination from point sources we excluded regions around each detected point source (Paper I) of radius 6 times the semimajor axis of the 1-σ encircled energy ellipse. The size of the large aperture was chosen to maximize signal-to-noise, whilst the individual annuli were chosen so as to contain in each approximately $\sim$1500 background-subtracted photons. This gave annuli with outer radii $0.07'$, $0.55'$, $1.4'$, $2.3'$ and $3.1'$. Appropriate count-weighted response matrices were generated for each spectrum, using the standard *CIAO* tools **mkrmf** and **mkwarf**. The spectra within each annulus were rebinned to ensure at least 20 photons in each spectral bin and to ensure a signal-to-noise ratio of at least 3.

We restricted our fitting to the energy-band 0.5–7.0 keV, on account of calibration uncertainties at lower energies and the steeply-rising background at high energies. At low energies, the background template spectrum becomes less reliable since there is known to be strong dependence in the soft X-ray background emission with pointing. We therefore took care to ensure that the data were truncated at low energies where the background and source began to converge. For the spectra of the two outermost annuli, this involved truncating the data below $\sim$0.7 keV; for the innermost annuli data were excluded below 0.5 keV. Care should be exercised when comparing results obtained for different energy bandwidths, as narrowing the bandwidth can introduce systematic uncertainties in the fitting. However, since the abundances were subsequently tied together in all annuli, we found that they were relatively unaffected by this procedure (Sect 4.5). We discuss the likely impact of uncertainties in the background in Sect 4.2.

3.1. *The large-aperture spectrum*

We modelled the spectrum with a hot gas component, a term to account for unresolved point-source emission and a component to accommodate the mild flaring. To model the hot gas, we adopted the APEC model of Smith et al. (2001), since it was the most up-to-date plasma code which is widely available (the impact of using a MEKAL model instead is addressed in Sect 4.3). To account for unresolved point-sources, we included a bremsstrahlung model with kT = 7.3 keV, which was found to give an excellent fit to the composite spectrum of the resolved sources (Paper I). To model the flaring, we used the parameterization adopted in Sect 2 for the flaring on the S3 chip, albeit with the normalization free. The components representing emission from the galaxy were additionally modified by photoelectric absorption due to cold material in the line-of-sight. The absorbing column was fixed at the Galactic value for the appropriate pointing (Dickey & Lockman 1990), and we adopted the absorption cross-sections of Morrison & McCammon (1983, but the results were unaffected if we adopted those of Bałucińska-Church & McCammon 1992).

We allowed Z_{Fe} to be free and initially tied the abundances of all remaining elements to Fe in their appropriate solar ratios. This model gave a good fit to the data (χ^2/dof=121.04/114), with $Z_{Fe}>$ 1.5. However, there were obvious sytematic discrepancies between the model and the data at low energies ($\lesssim$0.7 keV). We experimented with adding an additional hot gas component at a different temperature and, alternatively, systematically freeing individual metal abundances. In practice, the low-energy residuals were only significantly reduced by freeing O, for which the improvement in χ^2 was $> 99.9\%$ significant, on the basis of an F-test. We obtained best-fit abundances of $Z_{Fe}=0.77^{+1.66}_{-0.32}$ and $Z_O/Z_{Fe}=0.23^{+0.32}_{-0.23}$, for a gas temperature of 0.57 ± 0.02 keV. The fit was excellent (χ^2/dof=106/113). We experimented with systematically freeing the remaining abundances. Although there was no significant improvement in the fit statistic following this procedure, we were able to estimate reasonable 90% confidence limits for the abundances of Ne, Mg, and Si (Table 1)[3]. The spectrum and best-fit model are shown in Fig 2. The lines of Ne, Mg and Si are clearly visible in the spectrum, and so it is unsurprising that we have been able to constrain their abundances. In order to minimize the number of variable parameters, we kept fixed the shapes of the flare and point-source model components. To determine the impact of this assumption on our error-bars, we additionally fitted the $3'$ aperture spectrum simultaneously with the flare and composite point-source spectra. Both the best-fit values and the error-bars were minimally affected by this procedure. We further investigate the impact of varying these components in Sect 4.

Although the low-energy residuals were substantially reduced by freeing Z_O, there was still some evidence of a feature at these energies (although, due to the good fit at higher energies, it was not reflected transparently in a poor overall χ^2 value). We found that adding an additional hot gas component (which we might expect given the temperature gradient observed in Sect 3.2) led to a statistically significant improvement in fit (at 99% significance, on the basis of an F-test). The quality of the fit was excellent (χ^2/dof=97/111). The temperatures of the two hot-gas components were found to be $0.33^{+0.06}_{-0.04}$ and $0.72^{+0.95}_{-0.15}$ keV (in good agreement with the range of temperatures seen over the temperature gradient; Sect 3.2). The best-fitting abundances are shown in Table 1, and clearly indicate $\sim$solar Fe abundance, and

[3] Note: since the abundances ratios of Ne, Mg and Si to Fe were all consistent with unity, we determined the confidence region for each one of these elements assuming the abundance ratios for the others were *exactly* unity. This step was necessary to obtain interesting constraints

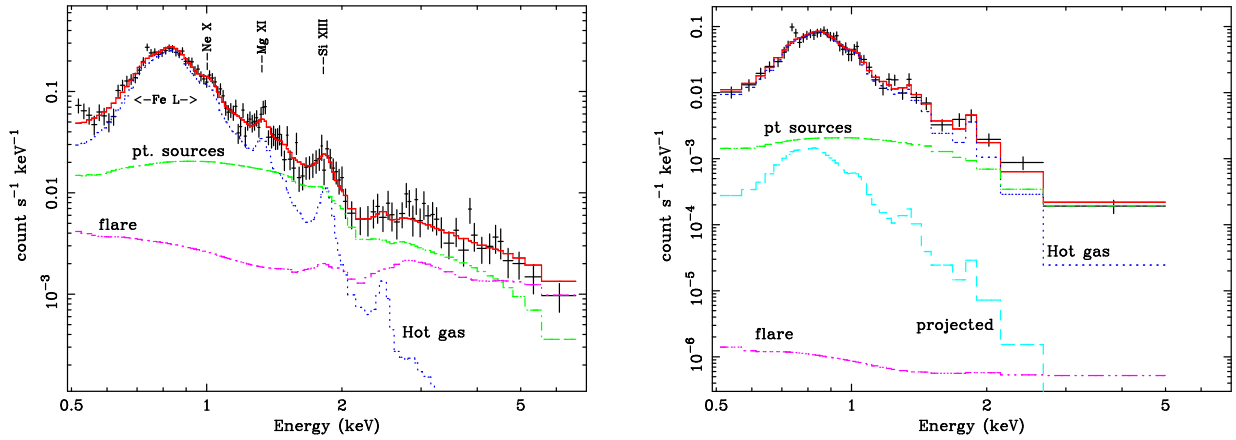

FIG. 2.— Left panel: spectrum of the large aperture. Right panel: spectrum of the innermost annulus. Also shown are the best-fit spectral-models (solid line; we use the single-temperature fit for the large aperture) and the individual contributions due to the hot gas (dotted line), the "contamination" due to projection effects (dashed line, right panel only), the unresolved point-sources (dash-dot line) and flaring (dash-dot-dot). The significance of the flaring component rises in the outermost annuli. Note that the feature at ∼0.72 keV in the left panel is too narrow to be an emission line; it is a statistical fluctuation at $< 3\sigma$ in a single data-bin. Since these spectra are not independent, it is visible in both panels, but it is not seen in other annuli.

TABLE 1
EMISSION-WEIGHTED ABUNDANCES WITHIN THE SINGLE 3′ (20 KPC) APERTURE

Model	Z_{Fe}	Z_O/Z_{Fe}	Z_{Ne}/Z_{Fe}	Z_{Mg}/Z_{Fe}	Z_{Si}/Z_{Fe}
0.5–7.0 keV					
1T	$0.77^{+1.66}_{-0.32}$	$0.23^{+0.32}_{-0.23}$	$1.21^{+0.55}_{-0.41}$	1.08±0.31	1.08±0.59
2T	1.09(>0.60)	0.02(<0.20)	···	···	···
0.4–7.0 keV					
1T	$1.10^{+2.18}_{-0.31}$	$0.34^{+0.29}_{-0.21}$	$1.21^{+0.53}_{-0.41}$	1.04±0.31	1.02±0.57
2T	>1.03	0.15 ± 0.14	···	···	···

NOTE. — Abundance measurements and 90% confidence intervals determined from fitting the large-aperture spectrum. We present both single temperature (1T) and two-temperature (2T) results for the bandpass 0.5–7.0 keV and 0.4–7.0 keV.

significantly sub-solar O. We experimented with allowing the remaining element abundances to vary, as for the single-temperature case. However, we found that none of the abundances (excepting Z_{Fe} and Z_O) could be constrained. Since adopting an over-simplistic spectral model can give rise to spurious abundances, we additionally tested the "power law DEM" (PLDEM) model of Buote et al. (2003a), in which the differential emission measure is a power law function of the temperature, and the power law exponent and range of gas temperatures are determined as fit parameters. The inferred abudances (Z_{Fe}>1.1) and (Z_O/Z_{Fe}< 0.22) were fully consistent with our two-temperature results. This agreement, which was also seen in NGC 5044 (Buote et al. 2003b), gives us confidence in the validity of the abundances derived from our two-temperature parameterization of the spectrum. This is further supported by the good agreement with the spatially-resolved analysis, below.

The ability to obtain reliable abundance measurements is critically dependent on our continuum emission constraints. Especially when there are multiple spectral components (i.e. hot gas, unresolved point sources and a flare component), it is essential to constrain the continuum at both ends of the spectrum. Below ∼0.5 keV, the spectrum is relatively free from strong emission lines, and so the data are extremely useful to this end. Unfortunately, the calibration of the *ACIS* chips is more uncertain in this regime, in part due to the build-up of carbanaceous deposits on the optical filter. Nevertheless, since we were using the most up-to-date correction for this quantum-efficiency degradation, we experimented with extending the bandpass down to 0.4 keV. Using either 1 or 2 temperature best-fit model for the 0.5–7.0 keV bandpass, we noticed a slight, systematic over-estimation of the count-rate below 0.5 keV (the discrepancy being more pronounced for the 2 temperature case). Fitting the data in the extended band, we found systematically higher values of Z_{Fe} and Z_O/Z_{Fe} for each model (Table 1), but the remaining abundance ratios were relatively unaffected. Although there are calibration uncertainties in this regime, we observed very similar behaviour using an AO1 observation of NGC 720 (Sect 5), for which the *ACIS* contamination was far less severe, which gave us confidence in these results.

3.2. *Spatially-resolved spectroscopy*

Observations of giant galaxies and groups often identify strong temperature gradients. In order to investigate any such effects, we performed spatially-resolved spec-

troscopy in a series of concentric annuli, centred on the peak of the X-ray emission. If there is a significant temperature gradient in the data, on account of the quasi-ellipsoidal distribution of the hot gas in the galaxy halo, the projection of the spectrum onto the sky does not accurately reflect the physical conditions at any point in the gas. In order to account for this effect, we employed the "onion-peeling" spectral deprojection algorithm outlined in Buote (2000a). To determine the extent to which such projection effects may alter our results, we additionally fitted traditional models directly to the spectra projected onto the sky. Henceforth we distinguish between projected and deprojected results by the soubriquets "2D" and "3D", respectively.

The quality of our data did not enable us to determine the metal abundance independently in each annulus, preventing our investigation of any abundance gradients. For the 2D fitting, to maximize our constraints on the data, we fitted the projected spectra simultaneously and tied equivalent metal abundances between each annulus. Since the magnitude of flaring did not vary strongly with position on the S3 chip (Sect 2), we were able to constrain the relative normalization of the flare component in each annulus to scale with the area of the extraction region, allowing only its total normalization to be fit. Since the fraction of emission arising from flaring differed in each annulus, this procedure enabled us to disentangle its contribution more effectively than for our large-aperture analysis (reflected in better constraints on our parameters). Analogously to our large-aperture fitting, we initially allowed Z_{Fe} to be fitted freely and tied the remaining elements to Fe in their appropriate solar ratios. To begin, we tested the hypothesis of no temperature gradient (i.e. tying the gas temperature between each annulus). This isothermal model gave $Z_{Fe} > 2.8$, but was statistically unacceptable (χ^2/dof=260.6/179). Freeing individual abundances did not enable an acceptable fit to be found, allowing us to reject the hypothesis of isothermality.

We obtained a statistically significant improvement in the fit (at >99.99% likelihood, on the basis of an f-test) if we allowed the temperature in each bin to be determined independently, although the fit was still unacceptable (χ^2/dof=217.6/175). Examination of the spectra revealed significant residuals at low energy, especially in the innermost annulus, analogous to those seen in the large aperture analysis. We therefore experimented with allowing the abundances of each metal in turn to be determined independently from Z_{Fe}, although significant improvements in the fit were only seen when O was freed (which fell to < 0.15). Adopting this model, we obtained a good fit to the data (χ^2/dof=189.4/174). We experimented with adding extra hot gas components to the fit to determine whether they led to significant improvements. However, we found no evidence of a significant change in either the abundances or the fit statistic. The best-fitting value for Z_{Fe} (shown in Table 2) was consistent with solar values (the lower limit at 99% significance on Z_{Fe} was 0.53). Furthermore, the gas was clearly deficient in O as compared to solar values; the 99% upper-limit on the Z_O/Z_{Fe} ratio was 0.24.

The temperature profile was relatively isothermal, excluding a small peak in the centre (Fig 3), although it was rather jagged in the second and third annuli. This is probably not a real effect; in fact kT in the outer two annuli is expected to be systematically high due to the truncation of the low-energy pass-band (Sect 4.5). Furthermore, due to the low temperature of the hot gas, the important O lines are blended to some extent with the Fe L-shell "hump". Since the shape of the "hump" strongly constrains the temperature, this produces some parameter degeneracy between Z_O and kT. As there were possible systematic errors in our determination of Z_O (Sect 4), we investigated the impact of such uncertainties by measuring the temperature profile with all elements tied to Fe. We found that the fit in this case was somewhat smoother, and the temperatures systematically higher (Fig. 3), although there was still evidence of a central temperature peak.

As for the single-temperature, large-aperture analysis, we next systematically freed individually the remaining abundances and determined appropriate confidence regions for the parameters. Although we did not find any evidence of an improvement in the fit statistic by this method, this simply reflects best-fitting abundance ratios with respect to Fe close to solar (at least for those elements which could be constrained). We found that we were able to constrain Si, Ne and Mg in addition to O and Fe. In contrast to our large-aperture analysis, we were able to obtain reliable confidence intervals when all of these metals were simultaneously freed. The best-fit abundances are shown in Table 2. It is interesting to note that the abundance ratios were somewhat better constrained than the absolute abundance of Fe. This is easily understood since the primary source of uncertainty on the abundances is our constraint on the continuum level. If the continuum is over-estimated, the equivalent widths of all the lines will be systematically under-estimated, and vice versa, producing a strong correlation between the abundances (manifesting itself in long, thin confidence regions in parameter space). We used a slightly modified implementation of the standard *Xspec* `vapec` model, in which the absolute abundance of Fe was directly determined, but for the other elements the fit parameters were the abundance *ratios* (in solar units) with respect to Z_{Fe}. This enabled us to measure directly the errors on the abundance ratios in *Xspec* without having explicitly to take account of this correlation. In previous studies (e.g. Buote et al. 2003b), we adopted Monte-Carlo simulations to achieve this.

For our 3D analysis, the inflated uncertainties in the profile introduced by the deprojection method were prohibitive if the metal abundances were to be determined by the fitting. We therefore fixed the metal abundances to the best-fit values obtained from 2D fitting and performed the deprojection using the algorithm outlined in Buote (2000a). To investigate the sensitivity of the temperature profile to our abundance determination, we additionally considered the case when $Z_O/Z_{Fe}= 1$. We found the results in both cases were very similar to equivalent results found for our 2D analysis (Fig 3). The temperatures tended to be a little higher in each annulus using 3D fitting, although this was most pronounced for the $Z_O/Z_{Fe}=1$ case, which cannot acceptably fit the spectra all annuli for either 2D or 3D fitting. In contrast, the deprojected model with free Z_O was able to give good fits in all annuli. The spectrum of the innermost bin and the best-fitting 3D model is shown in Fig 2. Since the tem-

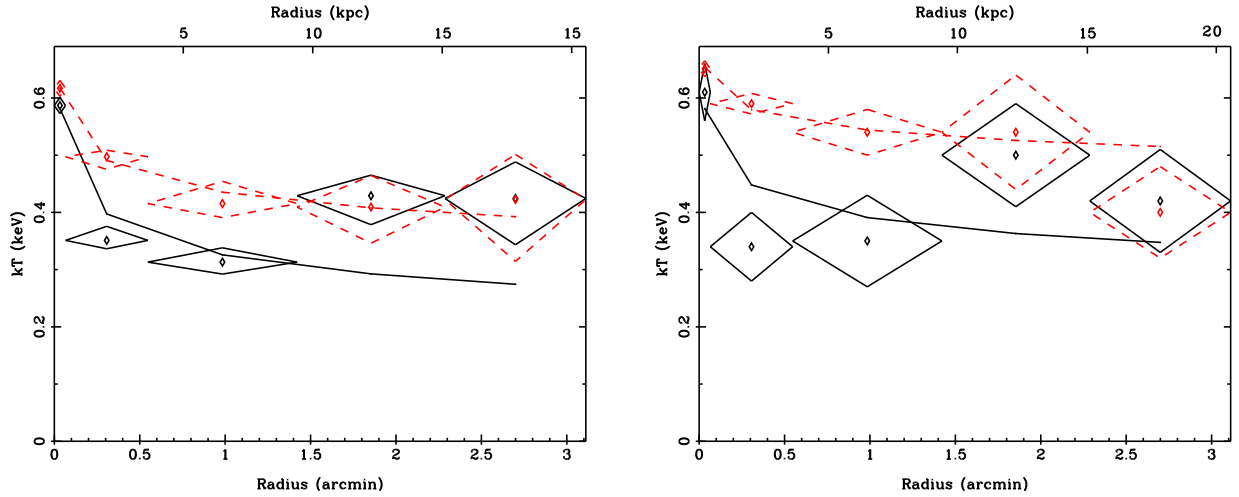

FIG. 3.— Left panel: the temperature profile determined by fitting the projected spectra. We show results determined both with all elements tied to Fe (dotted-lines) and with Z_O free (solid line). In addition, we show a best-fit power law model to the profile. Right panel: the same results, except fitting the deprojected spectra. For the deprojected analysis, it was necessary to fix Z_{Fe} and Z_O values at their best-fit values.

perature profile was relatively flat (excepting the innermost bin), projection effects were not especially important. In the innermost bin, where there is a temperature gradient, due to the relatively small spectral extraction region projection effects were also minor (Fig 2).

4. SYSTEMATIC ERRORS

In order to estimate the magnitude of any systematic errors on our data-analyis, we considered explicitly a number of effects, which are discussed in detail here. Those readers uninterested in the technical details can proceed directly to Sect 5. A summary of the magnitudes of each systematic effect is given in Table 2. The discussion herein focuses primarily on our simultaneous 2D spatially-resolved spectroscopy results, since they gave us the best constraints.

4.1. *Calibration issues*

A number of aspects of the satellite calibration may have possible systematic effects on our best-fit results. Using the standard *CIAO* data-processing software it was not possible to correct S3 chip data for "charge transfer inefficiency" (CTI), which degrades the spectral resolution of the data. We were, however, able to correct for a systematic drift in the instrumental gain by applying the `apply_gain`[4] task to our data An alternative procedure which allows compensation for the effects of CTI was proposed by Townsley et al. (2002)[5], although the calibration for this method is far less up-to-date. Using the CTI-corrected data (without the gain-correction), we accumulated spectra in a set of concentric annuli to match our spatially resolved spectroscopy. We obtained a good fit (χ^2/dof=184.1/173) with the same spectral model, but with systematically lower overall Fe abundance ($Z_{Fe}=0.79^{+1.06}_{-0.26}$). Of the abundance ratios, only Z_O/Z_{Fe} was significantly altered (becoming $0.33^{+0.23}_{-0.14}$). We obtained a very similar temperature profile to that found for our standard analysis, although the central peak was less pronounced ($kT=0.56^{+0.02}_{-0.08}$keV). It is difficult to disentangle to what extent the change in the best-fit abundances arose from the effects of the CTI correction, and to what extent they were simply a product of the less up-to-date calibration of this technique. Nonetheless, these values give an estimate of the calibration uncertainty due to the failure to correct for CTI.

It is also interesting to compare the results obtained for different releases of the *Chandra Caldb*; processing the data using version 2.25, for which the S3 spectral responses are known to have been subject to a small systematic error led to systematically higher values of Z_{Fe} and Z_O/Z_{Fe} ($\Delta Z_{Fe}\simeq0.2$ and $\Delta Z_O/Z_{Fe}\simeq0.15$). We can also use this discrepancy as a rough estimate of the magnitude of any possible calibration uncertainties remaining.

4.2. *The background templates*

A potentially serious source of error in the determination of metal abundances is an uncertainty in the background. Since the soft X-ray background is known to exhibit some dependence on the pointing, there were possible systematic errors in our background estimation at low energies (the background template was found to match our observation well at high energies). In order to determine the extent to which background errors may be affecting our results, we simply experimented with altering the background normalization by ±15%, comparable to the 10% variation between background fields found by M. Markevich[6]. The best-fit metal abundances and temperature profiles showed no significant changes due to this procedure (Table 2), and the confidence intervals were not appreciably affected. Our results, therefore, were relatively insensitive to errors in the background estimation.

4.3. *The plasma codes*

In order to investigate the extent to which the choice of plasma code model can influence our results, we ex-

[4] http://cxc.harvard.edu/cont-soft/software/corr_tgain.1.0.html
[5] http://cxc.harvard.edu/cont-soft/software/ACISCtiCorrector.1.37.html
[6] see http://cxc.harvard.edu/contrib/maxim/acisbg/COOKBOOK

TABLE 2
Abundance measurements and error budget

Par.	value	ΔStat.	Δcalib	Δbkd	Δcode	Δflare	Δbandw.	Δsources	$\Delta N_{\rm H}$
Z_{Fe}	1.10	$^{+1.7}_{-0.4}$	±0.3	±0.02	−0.16	±0.02	±0.33	−0.10	±0.01
Z_O/Z_{Fe}	0.05	$^{+0.10}_{-0.05}$	+0.3	±0.01	−0.02	±0.01	+0.11	±0.01	±0.01
Z_{Ne}/Z_{Fe}	0.99	±0.20	±0.1	±0.03	−0.03	±0.02	±0.03	±0.01	±0.02
Z_{Mg}/Z_{Fe}	1.07	±0.27	±0.08	±0.02	+0.33	±0.06	±0.04	+0.03	±0.02
Z_{Si}/Z_{Fe}	0.94	±0.53	±0.15	±0.05	+0.18	±0.03	±0.06	+0.05	±0.02

Note. — Emission-weighted abundance measurements for the spatially-resolved spectroscopy, fitting a single-temperature model for the hot gas as a function of radius. In addition to the statistical (Stat.) errors, we present an estimate of the possible magnitude of uncertainties on the abundances due to calibration (calib), background (bkd), plasma code (code), flare model (flare), bandwidth (bandw.), unresolved source spectrum (sources) and $N_{\rm H}$. It is difficult to assess the impact of multiple sources of systematic error *simultaneously* affecting our results (and it certainly is not correct simply to combine the errors in quadrature), so it is probably most correct to assume that the source of the largest systematic error dominates the systematic uncertainties. The magnitudes of the systematic errors listed are the changes in best-fit values, which were often more sensitive to such errors than the confidence regions (see text).

perimented with replacing the APEC hot gas model with a MEKAL (Mewe et al. 1985; Liedahl et al. 1995) component, since the atomic physics, particularly of the Fe L-shell line, is somewhat different. In general, both models were able to fit the data, although MEKAL gave systematically poorer χ^2 values (for example, the best-fit χ^2/dof for our best simultaneous fit to the spatially resolved spectra was 202.2/174, as compared to 189.4/174 for the APEC model).

We consistently obtained Fe abundances which were ∼10–20% lower with the MEKAL code (and a similar effect with the Z_O/Z_{Fe} value, although this was poorly-defined due to the large error-bars).The best-fit MEKAL abundances for this fit were $Z_{Fe}=0.94^{+2.8}_{-0.42}$ and $Z_O/Z_{Fe}=0.01^{+0.19}_{-0.01}$. Freeing up other abundances, we found good agreement with the APEC results for Ne and Si. However, Z_{Mg}/Z_{Fe} was systematically higher (1.43 ± 0.40), although marginally consistent within error-bars with the APEC result. Buote et al. (2003b) noted a systematic discrepancy of ∼10–20% between the shapes of the APEC and MEKAL spectral codes, in the vicinity of the Fe L-shell lines. This effect resulted in $Z_{Fe}^{apec} > Z_{Fe}^{mekal}$ for single-temperature fits, exactly as observed for NGC 1332. Since the Mg lines are close to the strong Fe L-shell lines (although, at the temperature of the system, they do not overlap), there is probably some interplay between them in the fit.

4.4. *The flaring background model*

In order to obtain formally acceptable spectral-fitting results, it was necessary to include a term to account for the residual flaring, even though we filtered the data carefully to remove the strongest flares. The flare was most evident above ∼2 keV and had uniform surface brightness across the interesting regions of the S3 chip. Since the spectral shape of the flare was not extremely well-constrained (due to the quality of the data) and since there were some discrepancies in its spectrum when estimated by two different means, this component was naturally a potential source of systematic errors. In order to determine the magnitude of any possible bias introduced by incorrect flare modelling, we investigated the effect of replacing our preferred model with the alternative one based on our S1 chip flare estimate. This gave a slightly worse fit (χ^2/dof=193.7/174) but there were no significant changes in the best-fit abundances, although the error-bar on Z_{Fe} was slightly widened so that the 90% upper-limit became 3.5. The best-fitting temperatures in each annulus were also not significantly changed by this procedure.

As a further test, we fitted the data by omitting completely any term to account for flaring. In the outermost annuli (where the contribution due to flaring is most significant due to the larger extraction area), the model significantly underestimated the data. Since the spectral shape of the flare is significantly harder than that of the unresolved point-source component, the unresolved emission term could not move to compensate entirely for the flaring contribution, so that the overall fit was formally unacceptable (χ^2/dof=227/175). Nonetheless, neither the best-fitting abundance values nor the confidence ranges associated with them were dramatically altered from our best-fit values ($\Delta Z_{Fe}\simeq \pm 0.3$, $\Delta Z_O/Z_{Fe}\simeq \pm 0.01$). Examination of the residuals to the fit indicated that the model had simply fitted at low energies at the expense of the data $\gtrsim$ 2 keV. The temperatures in all annuli were consistent, within error-bars, with the best-fitting 2D solution. However, the temperature was systematically lowered (by ∼0.05 keV and 0.1 keV) in the outermost two annuli, respectively. Nonetheless, our abundance measurements appear relatively insensitive to the modelling of the flare.

4.5. *The bandwidth*

The ability of the spectral-fitting models to determine reliable metal abundances and temperatures is dependent to some extent upon the bandwidth used in fitting (see Buote 2000a). In order to investigate the impact of narrowing our bandwidth, we first experimented by truncating the data above 2.0 keV. Such a procedure may be adopted to remove data heavily-biased by flaring, rather than the modelling we used. In adopting this procedure, we found that (omitting a flaring model component), we were able to obtain a good fit to the data (χ^2=158.2/152). There were no significant changes in the best-fitting abundances or the temperature profile con-

sidering the size of the statistical error-bars. As might be expected, however, this procedure dramatically increased our error bars on the absolute metal abundances; the upper limit on Z_{Fe} was no longer constrained, although the lower limit was not dramatically altered. The strong Fe L-shell lines in the 0.7–1.2 keV region play a vital role in determining both the temperature and the Fe abundance of the gas, and so it is unsurprising that we were still able to obtain a reliable gas temperature. However, since we did not have the higher-energy information, we were less able to constrain the continuum, hence the poorer constraints on our parameters.

In order to investigate the impact of our low-energy energy-cut, alternatively we truncated the data below 0.7 keV and re-fitted the models. In this case, we found a downward shift in the best-fit iron abundance, but the predominant effect was to degrade significantly the error-bars on our results; we found that $Z_{Fe} \geq 0.39$ and $Z_O/Z_{Fe} \leq 0.61$. The strongest relevant O lines are found at ∼0.5–0.8 keV, so it is hardly surprising that removing the data at low energies reduced our ability to constrain the O abundance. The low-energy data were also critical in enabling us to constrain the continuum level, especially as there were multiple components being fitted in each annulus. Failing to constrain the continuum translates into poorly-determined metal abundances since it introduces serious uncertainties into the determination of line equivalent widths. Furthermore, the temperature profile was smoothed somewhat by this procedure, predominantly through an increase in the best-fitting temperature in the third annulus (kT∼0.38 keV) and a slight widening of the error-bars. Since we were forced to exclude data below ∼0.7 keV in the outer two annuli during our analysis, this effect can explain the apparent "jaggedness" of the temperature profile in these data-bins. The best-fit abundances will not have been as strongly affected by our truncating the bandwidth in these annuli (as is confirmed by the agreement between the two-temperature single aperture fit and the spatially-resolved analysis), since the abundances were tied between all the annuli.

Since the background began to dominate the data at energies <0.5–0.7 keV, depending on the annuli, it was not possible to extend the bandwidth downwards in our annuli spectra to determine the impact of this procedure. However, for our large aperture extraction, it was possible to extend the bandwidth to 0.4 keV (although the calibration of the S3 chip is much more uncertain in this regime), as discussed in Sect 3.1. This increased the measured Z_{Fe} and Z_O/Z_{Fe} values somewhat (a similar effect was seen by Buote et al. 2003b), although the other abundance ratios were relatively unaffected.

4.6. *The unresolved source component*

We included a component to account for unresolved point-source emission in our data. The composite spectrum of all the resolved point sources in the D_{25} region of NGC 1332 could be fitted very well by a single bremsstrahlung model with temperature of 7.3 keV (see Paper I). Although this is in excellent agreement with observations of other early-type galaxies (Irwin et al. 2003), the spectra of fainter LMXB (which would be unresolved) tend to be somewhat harder than those of brighter objects (e.g. Church & Bałucińska-Church 2001). This

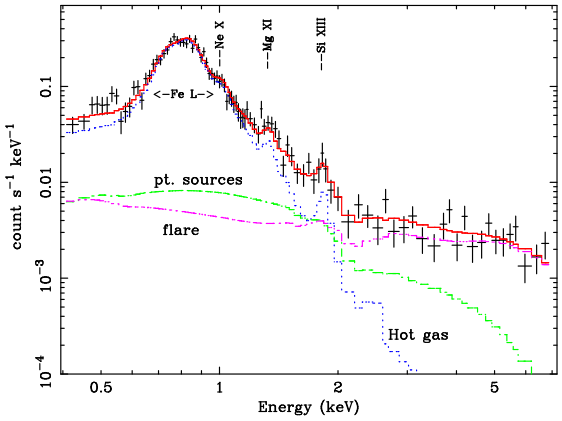

FIG. 4.— The best-fitting spectrum to the innermost annulus (0–0.9′; 0–7.1 kpc) of the NGC 720 data. The data are shown, along with the best-fitting model. We also show the spectrum decomposed into each component; the hot-gas (APEC) model is shown as a dotted line, the unresolved point-source component (bremsstrahlung) is shown as a dot-dash line. The flare component is shown with a dash-dot-dot line.

discrepancy is likely to be exacerbated if high/ soft-state black-hole binaries are more common amongst the brightest source population of a galaxy. To determine the sensitivity of our abundance measurements to the precise shape of this component, we next allowed the temperature of the bremsstrahlung term to fit freely. We found that its temperature tended to increase (although, due to the limited band-width of our spectra, it could not be constrained). The resulting temperature profile and abundances were in good agreement, within errors, with our best-fitting values.

4.7. *Column-density variation*

In our fitting, we fixed the neutral hydrogen column density to the canonical Galactic value estimated for the particular pointing (Dickey & Lockman 1990). In order to investigate any possible systematic effects arising from a mis-estimation of this value, we additionally fitted the data but allowed the N_H to fit freely. The best-fitting column-density, $N_H = (2.9^{+9.3}_{-2.5}) \times 10^{20}$ cm^{-2}, was in excellent agreement with our adopted canonical value ($N_H = 2.2 \times 10^{20}$ cm^{-2}) and we did not find any significant improvement in the fit statistic ($\Delta\chi^2$=0.1) by allowing N_H to be free. Since our best-fit N_H was so close to the canonical value, we found that freeing N_H had no significant effect on the metal abundance or temperature profile determination.

5. THE METALLICITY OF NGC 720

NGC 720 is a very isolated, moderate-L_X elliptical galaxy with a slightly higher L_X/L_B than NGC 1332 and significant hot gas emission. Since it was observed by *Chandra* during AO1, it provides an excellent opportunity to investigate metal abundances in another moderate L_X/L_B system. Buote et al. (2002) reported *Chandra* analysis results for NGC 720, in which they were able to place tight constraints upon the shape of the dark matter halo. Unfortunately, there were strong periods of flaring in the background during the observation, heavily contaminating the spectrum of the diffuse gas at energies $\gtrsim$2.0 keV. Since detailed spectral modelling

was not required in their analysis, these authors were able to mitigate against the effects of flaring by truncating the spectrum above 2 keV. With such a truncated energy-band, it was, however, not possible to constrain the metal abundances (c.f. Sect 4.5). We re-analyzed the *Chandra* data of NGC 720, adopting the techniques described in Sect. 2 to estimate the spectrum of the flare from the S3 chip. The data were reprocessed identically to NGC 1332, and the periods of the strongest flaring were removed, giving a total exposure of 29.3 ks. The flare spectrum could be parameterized adequately using the same model (broken power law plus broad gaussian line) as used for NGC 1332. Although the fit was not formally acceptable (χ^2/dof=234.4/196), the residuals predominantly appeared to be associated with low-amplitude, narrow features in the spectrum, so that the parameterization was a good approximation to the overall flare shape. Since the flaring dominated the spectrum only over a small number of energy bins (at the highest energy), such features were relatively unimportant, and our failure to account for them simply degraded the χ^2 slightly.

We extracted spectra from three annuli (with outer radii $0.9'$, $1.7'$ and $2.4'$) and centred at the X-ray centroid, computed in the same manner as for NGC 1332. The annuli were chosen to contain approximately the same number of photons, and extended out to $2.4'$; we did not extend the annuli out further since the data were there very heavily contaminated by background flaring. We fitted the data simultaneously in the range 0.5–7.0 keV, with a model comprising a term for the hot gas (APEC), a term to account for unresolved point source emission (a 7.3 keV bremsstrahlung component), and the flare model. We found there was little difference in the quality of the fit if we allowed the temperatures to be determined separately or if they were tied between each annulus, and so we tied the temperatures to improve our abundance and temperature constraints. Similarly, we tied the metal abundances between each annulus so as to determine an emission-weighted average. We initially tied all the metal abundances to Z_{Fe}, in their appropriate solar ratios, but we obtained a marginally unacceptable fit (χ^2/dof=400.0/345). We next experimented with allowing each metal in turn to fit freely of Fe, and found a statistically significant improvement in the fit only if the O was fitted freely. We obtained a good fit to the data (χ^2/dof=368.2/344) and the abundances were found to be $Z_{Fe}=0.47^{+0.36}_{-0.13}$ and $Z_O/Z_{Fe}=0.07^{+0.28}_{-0.07}$ and kT=0.55±0.02 keV

Next, exactly as for the large aperture analysis of NGC 1332, we experimented with extending the bandwidth down to 0.4 keV, as the count-rate was still significantly in excess of the background in each annulus at these energies. Since NGC 720 was observed during AO1, the degradation of the quantum efficiency at low energies was a less significant effect and so the calibration of the S3 chip in this range should be more secure. As in NGC 1332, we found that our best-fit to the 0.5–7.0 keV band slightly overestimated the continuum between 0.4–0.5 keV (thereby leading to an under-estimate of the metal abundances). Fitting the model to the extended pass-band data, we obtained a good fit (χ^2/dof=383.4/357) and somewhat higher metal abundances, but consistent with the errorbars of the restricted energy-range solution. We determined $Z_{Fe}=0.71^{+0.40}_{-0.21}$ and $Z_O/Z_{Fe}=0.23 \pm 0.21$, and kT=0.55±0.02. The lower-limit on Z_{Fe}, at the 99% confidence limit, was $Z_{Fe}=0.47$. We experimented with freeing the remaining abundances, but were only able to obtain constraints on Ne and Mg ($Z_{Ne}/Z_{Fe}=0.44 \pm 0.43$, $Z_{Mg}/Z_{Fe}=1.26 \pm 0.35$). The strong flaring at high energies largely swamped the data in the vicinity of the Si line, so that, in contrast to NGC 1332, we could not obtain Z_{Si}/Z_{Fe} constraints. The best-fitting spectrum for the innermost annulus is shown in Fig. 4. These results were in general agreement with our results for NGC 1332 (with the possible exception of the Z_{Ne}/Z_{Fe} ratio, which was ∼solar in NGC 1332, although the disagreement is marginal), and strongly excluded very sub-solar metal abundances except for O, for which Z_O∼0.2.

6. DISCUSSION

The *Chandra* observations of the normal, isolated, lenticular galaxy NGC 1332 enabled us to place constraints on the metal abundances and the temperature profile of the hot gas. Revisiting the *Chandra* data of the isolated elliptical NGC 720 we were also able to place good constraints on temperature and the metal abundances. The temperature profile of NGC 1332 was relatively isothermal, excepting a slight temperature peak in its centre. For NGC 720, we found that the data similarly showed evidence of an ∼isothermal profile. In neither case did we see convincing evidence of a central temperature dip, such as is seen in "cool core" clusters and groups. Both of these are normal, relatively isolated galaxies with moderate values of L_X/L_B, allowing us to investigate the enrichment of early-type galaxies in a regime between bright, gas-rich ellipticals (for which ∼solar abundances are typically being found; see introduction) and the very gas-poor galaxies in which very low abundances are still being reported.

6.1. *Near-solar Fe abundances*

In both of these galaxies, we were able to exclude the possiblity of the highly sub-solar Fe abundances often reported for early-type galaxies in the literature. These abundances were frequently subject to the "Fe bias", on account of fitting a single temperature model to intrinsically non-isothermal data (c.f. Buote 1999). Multiple temperature components in a spectrum may arise from a strong temperature gradient over the spectral extraction region or the mixing of photons due to projection effects (for 2D analysis). Alternatively, they may indicate a truly multiphase medium. We note that the hard component due to unresolved X-ray point sources in many early-type galaxies is too dissimilar spectrally to the hot gas to induce the "Fe bias". The presence of more than one spectral component in the single aperture spectrum of NGC 1332 can clearly be understood in terms of the slight temperature gradient (which is not so large as to require deprojected analysis) evident in our spatially-resolved results. This is supported by the good agreement between our single-temperature spatially-resolved and two-temperature single aperture abundances. The ability of of a two-temperature model to parameterize a temperature gradient in the observing aperture, and still yield reliable abundances, is an established effect (see

e.g. Buote et al. 2003b). It is possible that the spectrum is somewhat more complicated than this picture. However, the general agreement between the PLDEM and the two-temperature fits in the single aperture, in addition to the agreement between the spatially-resolved and single aperture fit results, suggest that the abundances are not especially sensitive to the precise parameterization, provided it contains more than a single temperature component in this region. Similar conclusions were reached by Buote et al. (2003b).

For the spatially-resolved spectroscopy of NGC 1332 and NGC 720, the lack of a strong temperature gradient (which removed the need for deprojection) and the fact that the fits were not improved appreciably by using more than one hot gas component indicate that these data were *not* subject to the Fe bias. In fact, similar modelling of the *ASCA* data simply gave rise to very poor abundance constraints ($Z_{Fe}> 0.3$ and $Z_{Fe}> 0.2$, respectively: Buote & Fabian 1998, correcting to the solar abundances of Grevesse & Sauval 1998). Interestingly, their best-fit *ASCA* values ($\sim$1.2 and $\sim$0.6) were in excellent agreement with our *Chandra* results. Multi-temperature modelling of low-L_X systems with *ASCA* or *Rosat* frequently gave similarly poor abundance constraints (e.g. Fabbiano et al. 1994), or were subject to parameter degeneracy in which erroneously low values of Z_{Fe} could be obtained (see Buote & Fabian 1998).

Our *Chandra* results, and similar results in the slightly lower-L_X/L_B radio galaxy NGC 1316 (Kim & Fabbiano 2003) now reveal a self-consistent picture of $\sim$solar abundances from the centres of cool core clusters down to these moderate L_X galaxies. This is in contrast, however, to the extremely sub-solar abundances which are still tending to be found in the lowest-L_X systems. If the low signal-to-noise of the data does not bias these low abundances, the lack of enrichment in the lower-mass systems is a significant challenge to our understanding of the chemical enrichment process. Although the $\sim$solar abundances found in NGC 1332 and NGC 720 are far more consistent with more massive groups and clusters, we still did not obtain the several times solar values of Z_{Fe} typically predicted by enrichment models for individual galaxies (e.g. Ciotti et al. 1991; Loewenstein & Mathews 1991; Brighenti & Mathews 1999).

6.2. *Abundance ratio implications for supernova enrichment*

A number of effects can enrich or dilute the hot gas in an early-type galaxy, such as supernovae, stellar mass-loss and gas inflow/ outflow (e.g. Matteucci & Greggio 1986). The α-elements are predominantly processed in supernovae and so the abundance ratios of these metals with respect to Fe provide a direct probe of the supernova enrichment history of the galaxy (e.g. Gastaldello & Molendi 2002). Mass loss from intermediate-mass stars is expected to contribute significantly to the ISM of an individual galaxy. However, assuming no nucleosynthesis of the α-elements in the envelopes of intermediate-mass stars, the abundance ratios of the ejected gas simply reflect the ISM make-up at the time the star formed. For enrichment dominated by very old stars, for example, stellar mass-loss will resemble type II supernovae, which were primarily responsible for the early enrichment.

In addition to Fe, we were able to obtain constraints for the abundance ratios of several other elements. Even taking into account the likely systematic effects observed in our data, the low Z_O/Z_{Fe} ratio we measure in both galaxies seems a robust result. Sub-solar values of Z_O/Z_{Fe} have been reported, using a variety of instruments, in a variety of other systems such as the bright group NGC 5044 (Buote et al. 2003b; Tamura et al. 2003), M 87 (Gastaldello & Molendi 2002), the massive elliptical NGC 4636 (Xu et al. 2002), the starbursting galaxy M 82 (Tsuru et al. 1997) and some clusters of galaxies (Loewenstein 2004, and references therein). We were also able to obtain constraints upon Mg, Ne and (for NGC 1332), Si. Intriguingly, we found that the Z_O/Z_{Mg} ratios were also significantly sub-solar. These elements are primarily produced during Type II supernovae, for which models tend to predict Z_O/Z_{Mg} $\sim$0.9–1.9 (Gibson et al. 1997, converting to the solar abundances of Grevesse & Sauval 1998). Similar discrepancies have been found in several systems (e.g. the centre of NGC 5044:Buote et al. 2003b; M 87: Gastaldello & Molendi 2002). In addition, in NGC 1332, the Z_O/Z_{Ne} ratio is also dramatically lower than predicted from Type II enrichment ($\sim$1.3–1.9; Gibson et al. 1997), which exacerbates the discrepancy in the Z_O/Z_{Mg} ratios. In NGC 720, the Z_O/Z_{Ne} ratio is closer to expectation, but the error-bars on the Ne abundance are large.

Since low abundance ratios for O have been seen in a variety of galaxies with different instruments, it is unlikely to relate to calibration uncertainties or any bias due to an abundance gradient (which we would not be able to constrain). SNe metal yields are highly sensitive to theoretical modelling, so perhaps the simplest explanation for our results is a problem with the SNe models considered. Loewenstein (2001) proposed that a significant contribution of hypernovae to the enrichment of gas in rich clusters could explain similar low values of Z_O/Z_{Fe} and Z_O/Z_{Si}, since the O-burning region is significantly enlarged in hypernovae. However, the hypernova models considered by Umeda et al. (2002) did not reproduce very low values of both Z_O/Z_{Mg} and Z_O/Z_{Ne}, as seen in our data, although the authors acknowledge that yields of Ne and Mg are sensitive to the assumptions of the model. It may be of interest to note that recent *Chandra* observations of the old SNR N49B revealed SN ejecta significantly enriched in Mg, apparently without accompanying Ne or O enrichment (Park et al. 2003).

Notwithstanding these reservations, we were able to place some constraints upon the relative contribution of SN Type Ia and Type II to the ISM enrichment. In order to compare with previous results, we performed fitting analogous to that of Gastaldello & Molendi (2002). Given the uncertainties in the hypernova yields, and to facilitate a meaningful comparison, we did not include any enrichment contribution from hypernovae. For a given fraction of enrichment arising from SNIa, f, theoretical metal yields from SNIa and SNII can be compared with the data. We used the SNIa models of Nomoto et al. (1997b), and the widely-adopted SNII yields taken from Nomoto et al. (1997a, hereafter N97). In addition, we also considered a range of SNII yields taken from Gibson et al. (1997, hereafter G97), in order to examine the impact of the SNII model choice on our results. It is worth noting that these models all assume a Salpeter IMF. Although variation in the IMF is not expected to affect

the abundance ratios as significantly as the overall abundances (Gibson et al. 1997), it remains a further source of systematic uncertainty.

For the SNII yields of N97, we obtained $f = 73 \pm 5\%$, which was relatively insensitive to the SNIa model chosen (since, of the relevant elements, only Si is significantly produced in SNIa, and the Si error bar is large). For the range of SNII models considered in G97, we found systematically lower enrichment fractions, reaching as low as $f = 39 \pm 10\%$. For NGC 720, we found similar results ($f = 85 \pm 6\%$ for the N97 model, and systematically lower values if G97 yields were used, reaching as low as $f = 62 \pm 12\%$). Due to our large abundance ratio error bars, it was not possible to distinguish convincingly between different SNIa and SNII models. One firm conclusion which we can draw, however, is that there is evidence of significant SNIa enrichment in both galaxies ($f \gtrsim 0.4$). Nevertheless, for comparison with other work, we adopt the N97 results as a standard, but caution that systematic discrepancies still exist between SNII models, which can significantly affect our results. It is interesting to compare our results with recent determinations of f$\sim$80–90% for the centre of M 87, using the same yields (Gastaldello & Molendi 2002). Similarly, in NGC 5044 Buote et al. (2003b) found f$\sim$70–80%, and f$\sim$80–90% was found in the centre of the bright nearby cluster A 1795 (Ettori et al. 2002). The good agreement with our results further confirms consistency in the enrichment mechanism stretching from cluster-scales to moderate-L_X galaxies.

Our fits to the data were, however, not formally acceptable for any mixture of SNIa and SNII model yields ($\chi^2/\mathrm{dof} > 4$). Examination of the fit residuals revealed that, as expected, the low value of Z_O/Z_{Fe} was problematic, even if we allowed the value for NGC 1332 to increase by $\sim$0.3, consistent with systematic uncertainties in its value. Uncertainties in the hypernova yields of Ne and Mg (Umeda et al. 2002) make it difficult to investigate similarly any putative hypernova contribution, which might account for the low Z_O/Z_{Fe} ratio. If, instead, the low Z_O/Z_{Fe} ratio reflects deficiencies in the SNII O yields, it may be sufficient simply to omit this data-point from the fitting. In this case we obtained good fits (albeit for only 2–3 data points), with a systematically lower f for both galaxies. For NGC 1332, f=$55 \pm 7\%$, using N97; using G97 it can be as low as $16 \pm 13\%$. For NGC 720 we found f=$68 \pm 8\%$ for N97, and systematically lower values down to $25 \pm 21\%$ for G97. In the centre of M 87 Gastaldello & Molendi (2002) also found a formally unacceptable fit; recomputing f based on their data, but omitting Z_O/Z_{Fe}, we obtained a good fit with f=$77 \pm 5\%$. In the case of NGC 5044, Buote et al. (2003b) computed f from the Si and S ratios, which were considered their most robust measurements, and so the low Z_O/Z_{Fe} ratio did not similarly affect the results. Therefore, even when O was excluded from the fitting, we found good agreement between our results for NGC 720 (and, to a lesser extent, NGC 1332) and these more massive systems. In NGC 1332, the slightly lower value of f may reflect the increased significance of stellar-mass loss (from old stars) in a lower-mass system.

We would like to think Bill Mathews and Fabrizio Brighenti for helpful discussions and carefully reading the manuscript. We would also like to thank Fabio Gastaldello and Aaron Lewis for helpful discussions concerning the data analysis and interpretation. This research has made use of the NASA/IPAC Extragalactic Database (*NED*) which is operated by the Jet Propulsion Laboratory, California Institute of Technology, under contract with the National Aeronautics and Space Administration. Support for this work was provided by NASA through *Chandra* award number G02-3104X, issued by the Chandra X-ray Observatory Center, which is operated by the Smithsonian Astrophysical Observatory for and on behalf of NASA under contract NAS8-39073. Partial support for this work was also provided by NASA under grant NAG5-13059, issued through the Office of Space Science Astrophysics Data Program.

REFERENCES

Anders, E. & Grevesse, N. 1989, Geochim. Cosmochim. Acta, 53, 197
Arimoto, N., Matsushita, K., Ishimaru, Y., Ohashi, T., & Renzini, A. 1997, ApJ, 477, 128
Bałucińska-Church, M. & McCammon, D. 1992, ApJ, 400, 699
Brighenti, F. & Mathews, W. G. 1999, ApJ, 515, 542
Buote, D. A. 1999, MNRAS, 309, 685
Buote, D. A. 2000a, ApJ, 539, 172
Buote, D. A. 2000b, MNRAS, 311, 176
Buote, D. A. 2002, ApJ, 574, L135
Buote, D. A. & Canizares, C. R. 1996, ApJ, 457, 177
Buote, D. A. & Fabian, A. C. 1998, MNRAS, 296, 977
Buote, D. A., Humphrey, P. J., & Canizares, C. R. 2004, in preparation. (Paper III)
Buote, D. A., Jeltema, T. E., Canizares, C. R., & Garmire, G. P. 2002, ApJ, 577, 183
Buote, D. A., Lewis, A. D., Brighenti, F., & Mathews, W. G. 2003a, ApJ, 594, 741
Buote, D. A., Lewis, A. D., Brighenti, F., & Mathews, W. G. 2003b, ApJ, 595, 151
Church, M. J. & Bałucińska-Church, M. 2001, A&A, 369, 915
Ciotti, L., Pellegrini, S., Renzini, A., & D'Ercole, A. 1991, ApJ, 376, 380
Davis, D. S. & White, R. E. 1996, ApJ, 470, L35+
Dickey, J. M. & Lockman, F. J. 1990, ARA&A, 28, 215
Ettori, S., Fabian, A. C., Allen, S. W., & Johnstone, R. M. 2002, MNRAS, 331, 635
Fabbiano, G., Kim, D.-W., & Trinchieri, G. 1994, ApJ, 429, 94
Gastaldello, F. & Molendi, S. 2002, ApJ, 572, 160
Gibson, B. K., Loewenstein, M., & Mushotzky, R. F. 1997, MNRAS, 290, 623
Grevesse, N. & Sauval, A. J. 1998, Space Science Reviews, 85, 161
Humphrey, P. J. & Buote, D. A. 2004, ApJ, in press, astro-ph/0402581 (Paper I)
Irwin, J. A., Athey, A. E., & Bregman, J. N. 2003, ApJ, 587, 356
Irwin, J. A., Sarazin, C. L., & Bregman, J. N. 2002, ApJ, 570, 152
Kim, D. & Fabbiano, G. 2003, ApJ, 586, 826
Kim, D.-W., Fabbiano, G., Matsumoto, H., Koyama, K., & Trinchieri, G. 1996, ApJ, 468, 175
Liedahl, D. A., Osterheld, A. L., & Goldstein, W. H. 1995, ApJ, 438, L115
Loewenstein, M. 2001, ApJ, 557, 573
Loewenstein, M. 2004, in Origin and Evolution of the Elements, from the Carnegie Observatories Centennial Symposia, eds. A. McWilliam & M. Rauch, CUP, 425
Loewenstein, M. & Mathews, W. G. 1991, ApJ, 373, 445
Loewenstein, M. & Mushotzky, R. F. 1998, in IAU Symp. 188: The Hot Universe, 53
Markevitch, M. 2002, astro-ph/0205333
Matsumoto, H., Koyama, K., Awaki, H., Tsuru, T., Loewenstein, M., & Matsushita, K. 1997, ApJ, 482, 133

Matsushita, K., et al. 1994, ApJ, 436, L41
Matteucci, F. & Greggio, L. 1986, A&A, 154, 279
Mewe, R., Gronenschild, E. H. B. M., & van den Oord, G. H. J. 1985, A&AS, 62, 197
Morrison, R. & McCammon, D. 1983, ApJ, 270, 119
Mulchaey, J. S. & Zabludoff, A. I. 1998, ApJ, 496, 73
Nomoto, K., Hashimoto, M., & Tsujimoto, T. 1997a, Nucl. Phys. A, 616, 79
Nomoto, K., Iwamoto, K., Nakasoto, N., Thielemann, F. K., Brachwitz, F., Tsujimoto, T., Kubo, Y., & Kishimoto, N. 1997b, Nucl. Phys. A, 621, 467
O'Sullivan, E. & Ponman, T. J. 2004, MNRAS, 349, 535
O'Sullivan, E., Vrtilek, J. M., Read, A. M., David, L. P., & Ponman, T. J. 2003, MNRAS, 346, 525
Park, S., Hughes, J. P., Slane, P. O., Burrows, D. N., Warren, J. S., Garmire, G. P., & Nousek, J. A. 2003, ApJ, 592, L41
Renzini, A. 1997, ApJ, 488, 35
Sambruna, R. M., Gliozzi, M., Donato, D., Tavecchio, F., Cheung, C. C., & Mushotzky, R. F. 2004, A&A, 414, 885
Sarazin, C. L., Irwin, J. A., & Bregman, J. N. 2001, ApJ, 556, 533
Smith, R. K., Brickhouse, N. S., Liedahl, D. A., & Raymond, J. C. 2001, ApJ, 556, L91
Tamura, T., Kaastra, J. S., Makishima, K., & Takahashi, I. 2003, A&A, 399, 497
Townsley, L. K., Broos, P. S., Nousek, J. A., & Garmire, G. P. 2002, Nucl. Instrum. Methods Phys. Res., 486, 751
Tsuru, T. G., Awaki, H., Koyama, K., & Ptak, A. 1997, PASJ, 49, 619
Umeda, H., Nomoto, K., Tsuru, T. G., & Matsumoto, H. 2002, ApJ, 578, 855
Xu, H., Kahn, S. M., Peterson, J. R., Behar, E., Paerels, F. B. S., Mushotzky, R. F., Jernigan, J. G., Brinkman, A. C., & Makishima, K. 2002, ApJ, 579, 600